Small-Signal Modeling and Controller Design Considerations for Dyna-C AC-DC Converter

Adrian Wiemer[†], Vishnu Mahadeva Iyer[‡], Arne Hinz[†], Subhashish Bhattacharya[‡], Rik W. De Doncker[†]

[†]Institute for Power Generation and Storage Systems (PGS) E. ON Energy Research Center, RWTH Aachen University
Aachen, Germany. Email: *adrian.wiemer@rwth-aachen.de, post_pgs@eonerc.rwth-aachen.de*
[‡] Future Renewable Electric Energy Delivery and Management (FREEDM) Systems Engineering Research Center,
North Carolina State University, 1791 Varsity Drive, NC 27606 Raleigh, USA. Email: *vmahade@ncsu.edu, sbhatta4@ncsu.edu*

***Abstract*—The Dyna-C ac-dc converter is a current-source-based topology featuring medium-frequency galvanic isolation. This paper presents the state-space based average and small signal modeling of Dyna-C ac-dc converter. A space vector based modulation strategy is developed, presented and validated by simulation. Based on the proposed small signal model for Dyna-C ac-dc converter, a two stage closed loop control approach is developed. The proposed approach comprises of an outer loop to regulate the transformer magnetizing-current and an inner *dq*-based vector control strategy for regulating the grid currents. Circuit simulation results are presented to validate the proposed models and the closed loop control scheme for the Dyna-C ac-dc converter.**

Index Terms*—ac-dc conversion, controller design, current-source converters, Dyna-C converter, small-signal modeling, vector control.

I. Dyna-C Converter

The Dyna-C converter [1], as shown in Fig. 1, consists of a current-source-based three-phase (3-ϕ) front-end converter, a medium-frequency single-phase flyback type transformer and a current-source-based H-bridge converter. Both, the front-end and H-bridge converters are realized using two-quadrant switches that conduct current in only one direction, but block voltages in both directions. This topology, capable of performing ac-dc power conversion, can handle bidirectional power flow. Current-source-based ac-dc converters are inherently buck rectifiers. Hence, compared to a voltage-source converter (VSC) based approach, a bulky line-frequency transformer or an additional dc-dc converter stage can be omitted to step down the grid voltage. This inherent buck characteristic of a current-source-based grid connected front-end of the Dyna-C converter ensures that the dc-link voltage applied to the magnetizing inductance L_m of the transformer is always less or equal to the line-to-line grid-voltage. Thus, the dc-link voltage of a Dyna-C is lower compared to that of a voltage-source-based active rectifier, which in turn results in lower insulation requirements for the dc-link. Another advantage of the current-source characteristic of the Dyna-C converter is its inherent short circuit handling capability. An accidental short circuit in a bridge leg does not affect the functionality of the converter, as the magnetizing inductance prevents the short circuit current from rising to destructive values. On the other hand, current-source-based converters are expected to have high reverse recovery and conduction losses due to the series connected diodes. In current-source-based converter systems, it is hard to achieve efficiency parity with conventional semiconductors based on Silicon (Si) semiconductor technology. However, with recent advances in Silicon Carbide (SiC) technology, it is possible to reduce the diode recovery losses in current-source converters [2] which will make current-source converter based systems competitive in efficiency to its voltage-source-based counterparts. Based on these considerations, the Dyna-C converter is a promising topology that enables reliable grid-connected ac-dc buck rectifiers with medium-frequency galvanic isolation for lower costs. A Dyna-C ac-ac converter is proposed in [1] as a 50 kVA three-phase solid-state transformer (SST) and as minimal topology for a bidirectional (SST) in [3]. Additional it can be utilized as a converter for instantaneous reactive power compensation [4]. In this paper, a detailed modulation scheme, a small-signal model and a closed-loop control scheme are presented and validated for a Dyna-C ac-dc converter. The paper is organized as follows. Section II discusses the modulation scheme for Dyna-C ac-dc converter. The state-space based average and small-signal models of Dyna-C converter are derived in Section III. Closed loop controller design considerations for the Dyna-C ac-dc converter are discussed in Section IV. The presented models and control strategy are validated through a comparission of switching and small singal model simulations in Section V.

II. Modulation Scheme for Dyna-C Converter

A Dyna-C converter modulation scheme is derived by a detailed analysis of its bridges switching states. In general a Dyna-C converter is operated like a flyback converter where the magnetizing inductor is first energized using the (3-ϕ) front-end bridge and then discharged by the H-bridge. The modulation scheme is based on three switching modes m_1, m_2 and m_3, which are applied for a fraction of the swiching period T_s, defined by duty cycles d_1, d_2 and d_3.

$$T_\mathrm{s} = (d_1 + d_2 + d_3)T_\mathrm{s} \tag{1}$$

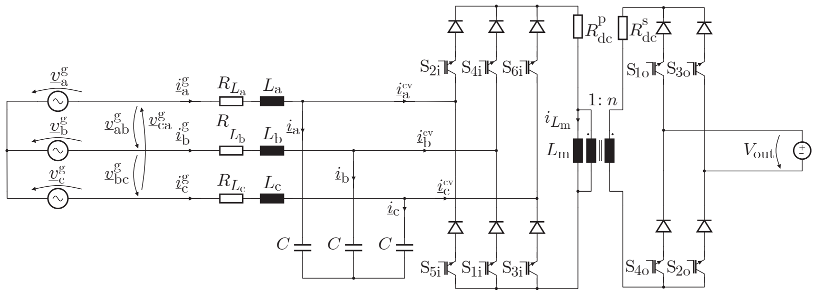

Fig. 1: Dyna-C topology with LC filter and transformer winding resistance

During modes m_1 and m_2, line-to-line voltages are applied across the magnetizing inductance, L_m as shown in Fig. 2a and 3a. In mode m_1 and m_2, the output dc voltage-source V_{out} is disconnected from the transformer as the H-bridge at the secondary side is not switched. In mode m_3, however, the 3-ϕ current-source front-end at the input is turned off.

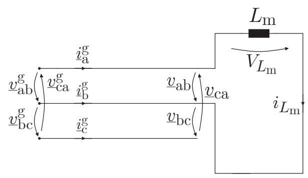

(a) Equivalent circuit - modulation mode m_1

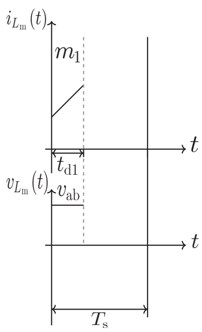

(b) Current and voltage waveform - modulation mode m_1

Fig. 2: Switching mode m_1 in sector 1

V_{out} is now connected to the transformer's secondary side using the H-bridge, so that it demagnetizes L_m. This behavior can be represented by the voltage-source in Fig. 4a. The three modes m_1, m_2 and m_3 are applied to control the magnetizing current i_{L_m} of the transformer [5]. The voltage pattern applied across L_m and the magnetizing current, i_{L_m} during the three operating modes are given in Fig. 2a to 4b. To develop a modulation scheme for a Dyna-C converter similar to a voltage-source converter [6], the fundamental cycle is divided into six sectors as in a typical current-source converter [5]. These sectors are defined in Table I and illustrated in Fig. 5. The individual sectors are placed according to the maximum absolute phase voltage of the grid, which results in an even division of the fundamental time period into 6 equal areas shown in Fig.5. The switching modes m_1, m_2 and m_3 given

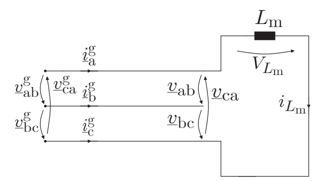

(a) Equivalent circuit - modulation mode m_2

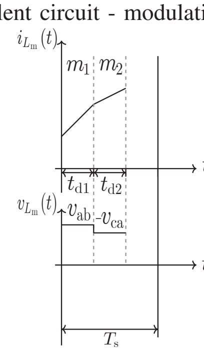

(b) Current and voltage waveform - modulation mode m_2

Fig. 3: Switching mode m_2 in sector 1

in Fig. 2a to 4b are valid in sector 1. For this sector according to [7] and [5] the duty cycles can be calculated by

$$d_1 = m_{\text{ind}} \cos(\theta + \frac{\pi}{6}) \tag{2}$$

$$d_2 = m_{\text{ind}} \cos(\theta - \frac{\pi}{2}) \tag{3}$$

$$d_3 = 1 - (d_1 + d_2) \tag{4}$$

where m_{ind} is the modulation index which is calculated by a fraction of absolute converter current i_d^{cv} and i_q^{cv} in dq frame, divided by the magnetizing current i_{L_m} and given by

$$m_{\text{ind}} = \frac{\sqrt{(i_d^{cv})^2 + (i_q^{cv})^2}}{i_{L_m}} \tag{5}$$

III. Modeling of Dyna-C Converter

A LC input filter, consisting of a capacitor and an inductance including its internal resistance, is used as depicted in Fig. 1 to limit the total harmonic distortion of the grid current. Further, the transformer winding resistances, R_{dc}^p and R_{dc}^s on

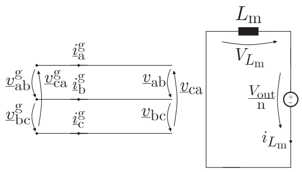

(a) Equivalent circuit - modulation mode m_3

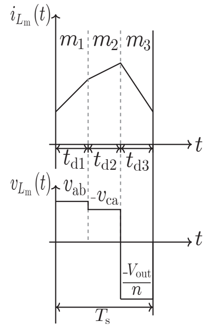

(b) Current and voltage waveform - modulation mode m_3

Fig. 4: Switching mode m_3 in sector 1

TABLE I: Definition of the six sectors in a fundamental cycle.

Switching Sector	Voltages
Sec$_1$	$v^\mathrm{g}_\mathrm{ab}(t) = \max(\lvert v^\mathrm{g}_\mathrm{ab}(t), v^\mathrm{g}_\mathrm{bc}(t), v^\mathrm{g}_\mathrm{ca}(t)\rvert)$
Sec$_2$	$-v^\mathrm{g}_\mathrm{ca}(t) = \max(\lvert v^\mathrm{g}_\mathrm{ab}(t), v^\mathrm{g}_\mathrm{bc}(t), v^\mathrm{g}_\mathrm{ca}(t)\rvert)$
Sec$_3$	$v^\mathrm{g}_\mathrm{bc}(t) = \max(\lvert v^\mathrm{g}_\mathrm{ab}(t), v^\mathrm{g}_\mathrm{bc}(t), v^\mathrm{g}_\mathrm{ca}(t)\rvert)$
Sec$_4$	$-v^\mathrm{g}_\mathrm{ab}(t) = \max(\lvert v^\mathrm{g}_\mathrm{ab}(t), v^\mathrm{g}_\mathrm{bc}(t), v^\mathrm{g}_\mathrm{ca}(t)\rvert)$
Sec$_5$	$v^\mathrm{g}_\mathrm{ca}(t) = \max(\lvert v^\mathrm{g}_\mathrm{ab}(t), v^\mathrm{g}_\mathrm{bc}(t), v^\mathrm{g}_\mathrm{ca}(t)\rvert)$
Sec$_6$	$-v^\mathrm{g}_\mathrm{bc}(t) = \max(\lvert v^\mathrm{g}_\mathrm{ab}(t), v^\mathrm{g}_\mathrm{bc}(t), v^\mathrm{g}_\mathrm{ca}(t)\rvert)$

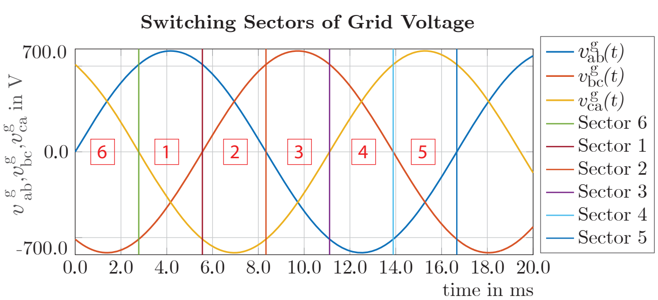

Fig. 5: Modulation scheme - sector definition.

the primary and secondary side of the transformer are also shown in Fig. 1. A balanced three-phase system is assumed for the analysis. The LC-filter parameters in Fig. 1 are set to the same value R, C and L for each phase. To derive an average model for the Dyna-C converter, the state-space averaging method is used [7], [8], where the state-space model for each switching mode introduced in the previous section are derived. The general space state model is calculated by

$$\frac{\mathrm{d}x(t)}{\mathrm{d}t} = Ax(t) + Bu(t) \tag{6}$$

The state-space matrix A and the input matrix B for the operating modes m_1, m_2 and m_3 within switching sector 1 are derived, considering the equivalent circuits given in Fig 2a, 3a and 4a. Note A and B are denoted by duty cycles d_1, d_2 and d_3 which correspond to modes m_1, m_2 and m_3 respectively. The state vector x and input vector u are defined as

$$x^T = \begin{bmatrix} i_{L_\mathrm{m}} & i^\mathrm{g}_\mathrm{a} & i^\mathrm{g}_\mathrm{b} & v_\mathrm{ab} & v_\mathrm{bc} \end{bmatrix} \tag{7}$$

$$u^T = \begin{bmatrix} \frac{V_\mathrm{out}}{n} & v^\mathrm{g}_\mathrm{ab} & v^\mathrm{g}_\mathrm{bc} \end{bmatrix} \tag{8}$$

For mode m_1 corresponding to sector 1, the following state matrix, A_d1 and input matrix, B_d1 are obtained

$$A_\mathrm{d1} = \begin{bmatrix} -\frac{R^\mathrm{p}_\mathrm{dc}}{L_\mathrm{m}} & 0 & 0 & -\frac{1}{L_\mathrm{m}} & 0 \\ 0 & -\frac{R}{L} & 0 & \frac{2}{3L} & \frac{1}{3L} \\ 0 & 0 & -\frac{R}{L} & -\frac{1}{3L} & \frac{1}{3L} \\ \frac{2}{C} & -\frac{1}{C} & \frac{1}{C} & 0 & 0 \\ -\frac{1}{C} & -\frac{1}{C} & -\frac{2}{C} & 0 & 0 \end{bmatrix} \tag{9}$$

$$B_\mathrm{d1} = \begin{bmatrix} 0 & 0 & 0 \\ 0 & -\frac{2}{3L} & -\frac{1}{3L} \\ 0 & \frac{1}{3L} & -\frac{1}{3L} \\ 0 & 0 & 0 \\ 0 & 0 & 0 \end{bmatrix} \tag{10}$$

During modes m_2 and m_3, the state matrices A_d2 and A_d3 and input matrices B_d2 and B_d3 are given in (11), (13) and (12), (14) respectively.

$$A_\mathrm{d2} = \begin{bmatrix} -\frac{R^\mathrm{p}_\mathrm{dc}}{L_\mathrm{m}} & 0 & 0 & -\frac{1}{L_\mathrm{m}} & -\frac{1}{L_\mathrm{m}} \\ 0 & -\frac{R}{L} & 0 & \frac{2}{3L} & \frac{1}{3L} \\ 0 & 0 & -\frac{R}{L} & -\frac{1}{3L} & \frac{1}{3L} \\ \frac{1}{C} & -\frac{1}{C} & \frac{1}{C} & 0 & 0 \\ \frac{1}{C} & -\frac{1}{C} & -\frac{2}{C} & 0 & 0 \end{bmatrix} \tag{11}$$

$$B_\mathrm{d2} = \begin{bmatrix} 0 & 0 & 0 \\ 0 & -\frac{2}{3L} & -\frac{1}{3L} \\ 0 & \frac{1}{3L} & -\frac{1}{3L} \\ 0 & 0 & 0 \\ 0 & 0 & 0 \end{bmatrix} \tag{12}$$

$$A_\mathrm{d3} = \begin{bmatrix} -\frac{R^\mathrm{s'}_\mathrm{dc}}{L_\mathrm{m}} & 0 & 0 & 0 & 0 \\ 0 & -\frac{R}{L} & 0 & \frac{2}{3L} & \frac{1}{3L} \\ 0 & 0 & -\frac{R}{L} & -\frac{1}{3L} & \frac{1}{3L} \\ 0 & -\frac{1}{C} & \frac{1}{C} & 0 & 0 \\ 0 & -\frac{1}{C} & -\frac{2}{C} & 0 & 0 \end{bmatrix} \tag{13}$$

$$B_\mathrm{d3} = \begin{bmatrix} \frac{1}{L_\mathrm{m}} & 0 & 0 \\ 0 & -\frac{2}{3L} & -\frac{1}{3L} \\ 0 & \frac{1}{3L} & -\frac{1}{3L} \\ 0 & 0 & 0 \\ 0 & 0 & 0 \end{bmatrix} \tag{14}$$

Resistor, $R_{\text{dc}}^{\text{s'}}$ is introduced which is R_{dc}^{s} in Fig. 1 referred to the primary side. Additionally, $R_{\text{dc}}^{\text{s'}} = R_{\text{dc}}^{\text{p}}$ is assumed for simplicity. The average state space matrix $\bar{A}_1$ and input matrix $\bar{B}_1$ are then calculated to

$$\bar{A}_1 = A_{\text{d1}}d_1 + A_{\text{d2}}d_2 + A_{\text{d3}}d_3 \tag{15}$$

$$\bar{B}_1 = B_{\text{d1}}d_1 + B_{\text{d2}}d_2 + B_{\text{d3}}d_3 \tag{16}$$

The averaged matrices given by (15) and (16) can be transfered into the dq domain by utilizing the dq transformation. By applying the state-space averaging method and the dq transformation in sector 1, the averaged state-space model for sector 1 can be calculated as

$$\bar{A}_{dq1} = \begin{bmatrix} -\frac{R_{\text{dc}}^{\text{p}}}{L_{\text{m}}} & 0 & 0 & -\frac{\alpha}{L_{\text{m}}} & \frac{\beta}{L_{\text{m}}} \\ 0 & -\frac{R}{L} & \frac{\text{d}\theta_{\text{f}}}{2\text{d}t} & \frac{1}{4L} & \frac{\sqrt{3}}{12L} \\ 0 & -\frac{\text{d}\theta_{\text{f}}}{2\text{d}t} & -\frac{R}{L} & -\frac{\sqrt{3}}{12L} & \frac{1}{4L} \\ \frac{\sqrt{3}\alpha}{2C} & -\frac{3}{4C} & \frac{\sqrt{3}}{4C} & 0 & \frac{\text{d}\theta_{\text{f}}}{2\text{d}t} \\ -\frac{\sqrt{3}\beta}{2C} & -\frac{\sqrt{3}}{4C} & -\frac{3}{4C} & -\frac{\text{d}\theta_{\text{f}}}{2\text{d}t} & 0 \end{bmatrix} \tag{17}$$

$$B_{dq1} = \begin{bmatrix} \frac{d_3}{L_{\text{m}}} & 0 & 0 \\ 0 & \frac{-1}{4L} & -\frac{\sqrt{3}}{12L} \\ 0 & \frac{\sqrt{3}}{12L} & -\frac{1}{4L} \\ 0 & 0 & 0 \\ 0 & 0 & 0 \end{bmatrix} \tag{18}$$

Further, the duty cycles d_1 and d_2 in (15) and (16) are replaced by expressions (2) and (3). Additionally, α and β in (17) and (18) are given by

$$\alpha = m_{\text{ind}}\cos(\Phi) \tag{19}$$

$$\beta = m_{\text{ind}}\sin(\Phi) \tag{20}$$

where m_{ind} is the modulation index intoduced earlier and Φ is the difference between the angular displacement θ_f of the dq reference frame d-axis and the angular displacement θ of the dq reference ac grid voltage, both to the real axis, which is illustrated in Fig. 6. As in [8], the same averaged dq state

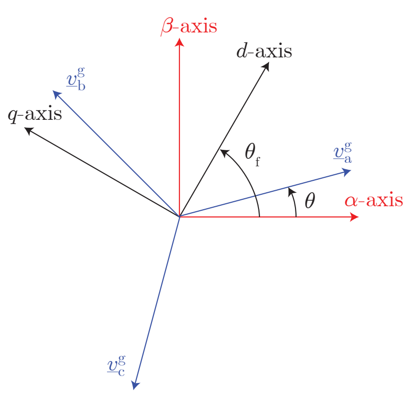

Fig. 6: dq reference frame and gird voltage v^{g} in the complex plane

matrix and input matrix can be obtained for each of the six switching sectors which yields

$$\bar{A}_{\text{dq}} = \bar{A}_{\text{dq1}} = \bar{A}_{\text{dq2}} = \bar{A}_{\text{dq3}} = \bar{A}_{\text{dq4}} = \bar{A}_{\text{dq5}} = \bar{A}_{\text{dq6}} \tag{21}$$

$$\bar{B}_{\text{dq}} = \bar{B}_{\text{dq1}} = \bar{B}_{\text{dq2}} = \bar{B}_{\text{dq3}} = \bar{B}_{\text{dq4}} = \bar{B}_{\text{dq5}} = \bar{B}_{\text{dq6}} \tag{22}$$

Therefore, the averaged state-space model can be formulated as

$$\frac{\text{d}x_{\text{dq}}}{\text{d}t} = \bar{A}_{\text{dq}}x_{\text{dq}} + \bar{B}_{\text{dq}}u_{\text{dq}} \tag{23}$$

Based on (23), the large and small-signal model can be calculated as in [8], by intoducing the follwing terms in (23)

$$x_{\text{dq}} = X_{\text{dq}} + \tilde{x}_{\text{dq}} \tag{24}$$

$$u_{\text{dq}} = U_{\text{dq}} + \tilde{u}_{\text{dq}} \tag{25}$$

Formulas (24) and (25) replace the averaged values by large and small-signal values. Based on this the large signal model is defined as

$$\frac{\text{d}X_{\text{dq}}}{\text{d}t} = \bar{A}_{\text{dq}}^{\text{L}}X_{\text{dq}} + \bar{B}_{\text{dq}}^{\text{L}}U_{\text{dq}} \tag{26}$$

The large signal state and input matrices, $\bar{A}_{\text{dq}}^{\text{L}}$ and $\bar{B}_{\text{dq}}^{\text{L}}$ are calculated to

$$\bar{A}_{\text{dq}}^{\text{L}} = \begin{bmatrix} -\frac{R_{\text{dc}}^{\text{p}}}{L_{\text{m}}} & 0 & 0 & -\frac{\alpha_{\text{L}}}{L_{\text{m}}} & \frac{\beta_{\text{L}}}{L_{\text{m}}} \\ 0 & -\frac{R}{L} & \frac{\omega_{\text{g}}}{2} & \frac{1}{4L} & \frac{\sqrt{3}}{12L} \\ 0 & -\frac{\omega_{\text{g}}}{2} & -\frac{R}{L} & -\frac{\sqrt{3}}{12L} & \frac{1}{4L} \\ \frac{\sqrt{3}\alpha_{\text{L}}}{2C} & -\frac{3}{4C} & \frac{\sqrt{3}}{4C} & 0 & \frac{\omega_{\text{g}}}{2} \\ -\frac{\sqrt{3}\beta_{\text{L}}}{2C} & -\frac{\sqrt{3}}{4C} & -\frac{3}{4C} & -\frac{\omega_{\text{g}}}{2} & 0 \end{bmatrix} \tag{27}$$

$$\bar{B}_{\text{dq}}^{\text{L}} = \begin{bmatrix} \frac{D_3}{L_{\text{m}}} & 0 & 0 \\ 0 & \frac{-1}{4L} & -\frac{\sqrt{3}}{12L} \\ 0 & \frac{\sqrt{3}}{12L} & -\frac{1}{4L} \\ 0 & 0 & 0 \\ 0 & 0 & 0 \end{bmatrix} \tag{28}$$

The large signal state and input vectors are specified as

$$X_{\text{dq}}^T = \begin{bmatrix} I_{\text{L}_{\text{m}}} & I_{\text{d}}^{\text{g}} & I_{\text{q}}^{\text{g}} & V_{\text{d}} & V_{\text{q}} \end{bmatrix} \tag{29}$$

$$U_{\text{dq}}^T = \begin{bmatrix} \frac{V_{\text{out}}}{n} & V_{\text{d}}^{\text{g}} & V_{\text{q}}^{\text{g}} \end{bmatrix} \tag{30}$$

where $\omega_{\text{g}} = \frac{\text{d}\theta_{\text{f}}}{\text{d}t}$. The terms in (19) and (20) are replaced by its corresponding large signal values

$$\alpha_{\text{L}} = M_{\text{ind}}\cos(\Phi) \tag{31}$$

$$\beta_{\text{L}} = M_{\text{ind}}\sin(\Phi) \tag{32}$$

The small-signal model is given by

$$\frac{\text{d}\tilde{x}_{\text{dq}}}{\text{d}t} = \bar{A}_{\text{dq}}^{\text{S}}\tilde{x}_{\text{dq}} + \bar{B}_{\text{dq}}^{\text{S}}\tilde{u}_{\text{dq}} \tag{33}$$

Further, the small-signal input matrix $\bar{B}_{\text{dq}}^{\text{S}}$ can be split into the control input matrix $\bar{B}_{\text{cont}}^{\text{S}}$ and the disturbance input matrix $\bar{D}_{\text{dist}}^{\text{S}}$, while the small-signal input vector $\tilde{u}_{\text{dq}}$ can be separated into the control input vector $\tilde{u}_{\text{cont}}$ and the disturbance input vector $\tilde{u}_{\text{dist}}$.

$$\bar{B}_{\text{dq}}^{\text{S}}\tilde{u}_{\text{dq}} = \bar{B}_{\text{cont}}^{\text{S}}\tilde{u}_{\text{cont}} + \bar{D}_{\text{dist}}^{\text{S}}\tilde{u}_{\text{dist}} \tag{34}$$

$\bar{B}_{\text{cont}}^{\text{S}}$, $\tilde{u}_{\text{cont}}$, $\bar{D}_{\text{dist}}^{\text{S}}$ and $\tilde{u}_{\text{dist}}$ are obtained as follows

$$\bar{A}^{\rm S}_{\rm dq} = \begin{bmatrix} -\frac{R^{\rm p}_{\rm dc}}{L_{\rm m}} & 0 & 0 & -\frac{\alpha}{L_{\rm m}} & \frac{\beta}{L_{\rm m}} \\ 0 & -\frac{R}{L} & \frac{\omega_{\rm g}}{2} & \frac{1}{4L} & \frac{\sqrt{3}}{12L} \\ 0 & -\frac{\omega_{\rm g}}{2} & -\frac{R}{L} & -\frac{\sqrt{3}}{12L} & \frac{1}{4L} \\ \frac{\sqrt{3}\alpha}{2C} & -\frac{3}{4C} & \frac{\sqrt{3}}{4C} & 0 & \frac{\omega_{\rm g}}{2} \\ -\frac{\sqrt{3}\beta}{2C} & -\frac{\sqrt{3}}{4C} & -\frac{3}{4C} & -\frac{\omega_{\rm g}}{2} & 0 \end{bmatrix} \tag{35}$$

$$\bar{D}^{\rm S}_{\rm dist} = \begin{bmatrix} \frac{D_3}{L_{\rm m}} & 0 & 0 \\ 0 & \frac{-1}{4L} & -\frac{\sqrt{3}}{12L} \\ 0 & \frac{\sqrt{3}}{12L} & -\frac{1}{4L} \\ 0 & 0 & 0 \\ 0 & 0 & 0 \end{bmatrix} \tag{36}$$

$$\bar{B}^{\rm S}_{\rm cont} = \begin{bmatrix} -\frac{(\cos(\Phi)V_{\rm d} - \sin(\Phi)V_{\rm q})}{L_{\rm m}} & \frac{\alpha_{\rm L}V_{\rm d} + \beta_{\rm L}V_{\rm q}}{L_{\rm m}} & \frac{V'_{\rm out}}{L_{\rm m}} \\ 0 & 0 & 0 \\ 0 & 0 & 0 \\ \frac{\sqrt{3}}{2C}I_{\rm L_m}\cos(\Phi) & -\frac{\sqrt{3}I_{\rm L_m}\beta_{\rm L}}{2C} & 0 \\ -\frac{\sqrt{3}}{2C}I_{L_{\rm m}}\sin(\Phi) & -\frac{\sqrt{3}I_{\rm L_m}\alpha_{\rm L}}{2C} & 0 \end{bmatrix} \tag{37}$$

The small-signal state and input vectors are defined as

$$\tilde{u}^T_{\rm cont} = \begin{bmatrix} \tilde{m}_{\rm ind} & \tilde{\phi} & \tilde{d}_3 \end{bmatrix} \tag{38}$$

$$\tilde{u}^T_{\rm dist} = \begin{bmatrix} \tilde{v}'_{\rm out} & \tilde{v}^{\rm g}_{\rm d} & \tilde{v}^{\rm g}_{\rm q} \end{bmatrix} \tag{39}$$

The derived large and small-signal model can be used to derive a controller topology and to model the dynamic behaviour of the Dyna-C converter.

IV. Closed Loop Control of Dyna-C Converter

The objective of a Dyna-C converter control system is to maintain the magnetizing current $i_{L_{\rm m}}$ according to its reference value, while drawing sinusoidal currents from the grid. A control block diagram can be derived based on the average state-space model given in (23). As in a current-soucre inverter a two loop control approach is used [7], consisting of an inner loop to control the dq grid currents $I^{\rm g}_{\rm d}$ and $I^{\rm g}_{\rm q}$ and an outer loop for the magnetizing current $I_{\rm L_m}$, which are indicated by the blue boxes in Fig. 7. To develop a controller topology, the inner loop is considered first. The aim is to obtain a control scheme with $I^{\rm g^*}_{\rm d}$ and $I^{\rm g^*}_{\rm q}$ as reference values. This is the reason for the second and third row of the state-space model in (27) and (28) to be choosen in order to derive a controller topology and rearranged to

$$V_{\rm d} = \underbrace{4L\frac{{\rm d}I^{\rm g}_{\rm d}}{{\rm d}t}}_{\rm Deriv.} + 4RI^{\rm g}_{\rm d} - \underbrace{2L\omega_{\rm g}I^{\rm g}_{\rm q}}_{\rm Cross\ coup.} + \underbrace{V^{\rm g}_{\rm d} + \frac{\sqrt{3}}{3}V^{\rm g}_{\rm q} - \frac{\sqrt{3}}{3}V_{\rm q}}_{V_{\rm e}} \tag{40}$$

$$V_{\rm q} = \underbrace{4L\frac{{\rm d}I^{\rm g}_{\rm q}}{{\rm d}t}}_{\rm Deriv.} + 4RI^{\rm g}_{\rm q} + \underbrace{2L\omega_{\rm g}I^{\rm g}_{\rm d}}_{\rm Cross\ coup.} + \underbrace{V^{\rm g}_{\rm q} + \frac{\sqrt{3}}{3}V_{\rm d} - \frac{\sqrt{3}}{3}V^{\rm g}_{\rm d}}_{V_{\rm f}} \tag{41}$$

According to [7] the derivative and cross coupling terms in (40) and (41) can be represented by

$$V_{\rm cd} = 4L\frac{{\rm d}I^{\rm g}_{\rm d}}{{\rm d}t} - 2L\omega_{\rm g}I^{\rm g}_{\rm q} \tag{42}$$

$$V_{\rm cq} = 4L\frac{{\rm d}I^{\rm g}_{\rm q}}{{\rm d}t} + 2L\omega_{\rm g}I^{\rm g}_{\rm d} \tag{43}$$

This can be reformulated to

$$V_{\rm cd} + jV_{\rm cq} = G_{\rm PI}(s)(I_{\rm cd} + jI_{\rm cq}) \tag{44}$$

where the controller transfer function in (44) is the modified PI controller transfer function,

$$G_{\rm PI}(s) = \frac{(k_{\rm p}s + j\omega) + k_{\rm I}}{s} \tag{45}$$

to obtain an equivalent voltage to current relation. Decomposing (44) into real and imaginary part and inserting it into (42) and (43) yields

$$V_d = \frac{k_{\rm p}s + k_{\rm I}}{s}I_{\rm cd} - \frac{k_{\rm p}\omega}{s}I_{\rm cq} + 4RI^{\rm g}_{\rm d} + V_{\rm e} \tag{46}$$

$$V_{\rm q} = \frac{k_{\rm p}s + k_{\rm I}}{s}I_{\rm cq} + \frac{k_{\rm p}\omega}{s}I_{\rm cd} + 4RI^{\rm g}_{\rm q} + V_{\rm f} \tag{47}$$

From (46) and (47) the currents to modulate the duty cycles are obtained by

$$I^{\rm cv}_{\rm d} = \omega CV_{\rm q} \tag{48}$$

$$I^{\rm cv}_{\rm q} = -\omega CV_{\rm d} \tag{49}$$

In (48) and (49), steady state is assumed and the grid current feed forward is neglected. The resulting control block diagram is depicted in Fig. 7. The duty cycle modulator depicted in Fig. 7 calculates duty cycles d_1 and d_2 of modes m_1 and m_2 using $I^{\rm cv}_{\rm d}$ and $I^{\rm cv}_{\rm q}$ are calculated by (5). From these duty cycles, the switching signals for switches in the input bridge (S_{1i} - S_{6i}) and the output bridge (S_{1o} - S_{4o}) of the Dyna-C are calculated by the 'sw signal modulator' in Fig. 7. To regulate the magnetizing current, $i_{L_{\rm m}}$, an outer control loop is added as shown in Fig. 7.

In order to design controller parameters, the small-signal model given by (35) - (39) can be utilized to derive the controller to output transfer functions. The effect of a single control input on a particular output is considered for deriving each transfer function. As an example, the effect of control input $\tilde{u}_1 = \tilde{m}_{\rm ind}(t) = \tilde{u}_{\rm cont}(1,1)$ on the output $\tilde{i}^g_d$ is evaluated to find the corresponding transfer function G_{11}. Therefore, the first column of (37) given by $\bar{B}_1 = \bar{B}^{\rm S}_{\rm cont}(n,1)$ where $n \in \{1,..,5\}$ is used as the input vector and the output vector $\bar{C}_1$ is set to

$$\bar{C}_1 = \begin{bmatrix} 0 & 1 & 0 & 0 & 0 \end{bmatrix} \tag{50}$$

The simplified state-space equation which can be utilized to derive this transfer function is given by

$$\frac{{\rm d}\tilde{x}_{\rm dq}}{{\rm d}t} = \bar{A}^{\rm S}_{\rm dq}\tilde{x}_{\rm dq} + \bar{B}_1\tilde{u}_1 \tag{51}$$

$$\hat{y}_{\rm dq} = \bar{C}_1\tilde{x}_{\rm dq} \tag{52}$$

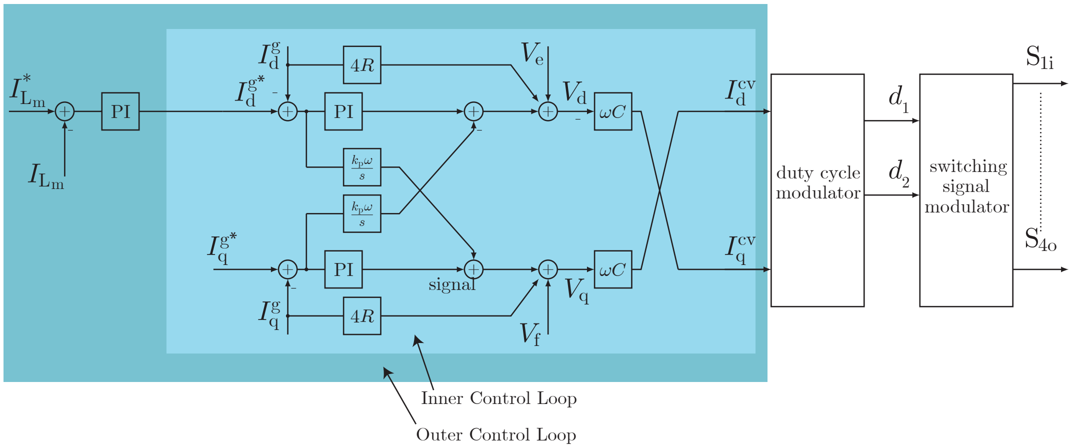

Fig. 7: Dyna-C control block diagram.

These time domain equations are transformed to the frequency domain to obtain

$$s\hat{X}_{\mathrm{dq}}(s) = \bar{A}^{\mathrm{S}}_{\mathrm{dq}}\hat{X}_{\mathrm{dq}}(s) + \bar{B}_1\hat{U}_1(s) \tag{53}$$

$$\hat{Y}_{\mathrm{dq}}(s) = \bar{C}_1\hat{X}_{\mathrm{dq}}(s) \tag{54}$$

Rearranging (53) and substituting it in (54) gives

$$G_{11}(s) = \frac{\hat{I}^{\mathrm{g}}_{\mathrm{d}}}{\hat{M}_{\mathrm{ind}}(s)} = \frac{\hat{Y}_{\mathrm{dq}}(s)}{\hat{U}_1(s)} = \bar{C}_1[sI - \bar{A}^{\mathrm{S}}_{\mathrm{dq}}]^{-1}\bar{B}_1 \tag{55}$$

The capitalized values in (55) represent Laplace domain quantities. To calculate G_{12} and G_{13}, the input vectors are set to $\bar{B}_2 = \bar{B}^{\mathrm{S}}_{\mathrm{cont}}(n,2)$ and $\bar{B}_3 = \bar{B}^{\mathrm{S}}_{\mathrm{cont}}(n,3)$, where $n \in \{1,..,5\}$. The control inputs are chosen to be $\tilde{u}_2 = \tilde{\phi}(t) = \tilde{u}_{\mathrm{cont}}(2,1)$ and $\tilde{u}_3 = \tilde{d}_3(t) = \tilde{u}_{\mathrm{cont}}(3,1)$ respectively, while the output vector $\bar{C}_1$ remains the same.

$$G_{12}(s) = \frac{\hat{I}^{\mathrm{g}}_{\mathrm{d}}(s)}{\hat{\phi}(s)} = \frac{\hat{Y}_{\mathrm{dq}}(s)}{\hat{U}_2(s)} = \bar{C}_1[sI - \bar{A}^{\mathrm{S}}_{\mathrm{dq}}]^{-1}\bar{B}_2 \tag{56}$$

$$G_{13}(s) = \frac{\hat{I}^{\mathrm{g}}_{\mathrm{d}}(s)}{\hat{\phi}(s)} = \frac{\hat{Y}_{\mathrm{dq}}(s)}{\hat{U}_3(s)} = \bar{C}_1[sI - \bar{A}^{\mathrm{S}}_{\mathrm{dq}}]^{-1}\bar{B}_3 \tag{57}$$

Transfer functions $G_{21}(s)$, $G_{22}(s)$ and $G_{23}(s)$ of current $\hat{I}^{\mathrm{g}}_{\mathrm{q}}$ are calculated by setting the output vector to

$$\bar{C}_2 = \begin{bmatrix} 0 & 0 & 1 & 0 & 0 \end{bmatrix} \tag{58}$$

Thus, the six transfer functions that relate the control inputs to the dq currents are given by

$$G_{11} = \frac{\hat{I}^{\mathrm{g}}_{\mathrm{d}}(s)}{\hat{M}_{\mathrm{ind}}(s)} \quad G_{12} = \frac{\hat{I}^{\mathrm{g}}_{\mathrm{d}}(s)}{\hat{\phi}(s)} \quad G_{13} = \frac{\hat{I}^{\mathrm{g}}_{\mathrm{d}}(s)}{\hat{D}_3(s)} \tag{59}$$

$$G_{21} = \frac{\hat{I}^{\mathrm{g}}_{\mathrm{q}}(s)}{\hat{M}_{\mathrm{ind}}(s)} \quad G_{22} = \frac{\hat{I}^{\mathrm{g}}_{\mathrm{q}}(s)}{\hat{\phi}(s)} \quad G_{23} = \frac{\hat{I}^{\mathrm{g}}_{\mathrm{q}}(s)}{\hat{D}_3(s)} \tag{60}$$

To validate the small-signal model, the follwoing assumptions are made. The angular displacement of the grid voltage and reference frame is set to $\Phi = 0$. This is justified because the grid voltage $v^{\mathrm{g}}_{\mathrm{a}}$ has its peak value at $t = 0$ and the dq transformation aligns the d axis with voltage $v^{\mathrm{g}}_{\mathrm{a}}$ [9], which is achieved in grid connected converters by a PLL [10]. Further, duty cycles d_1, d_2 are related to the modulation index $\tilde{m}_{\mathrm{ind}}$ as given by (2) and (3), why the dynamics in $\tilde{m}_{\mathrm{ind}}$ are coupled to d_3, which can be expressed by the other duty cycles as shown earlier in (4). Under these assumptions the converter dynamics between $\tilde{m}_{\mathrm{ind}}$ and the grid currents $\tilde{i}^{\mathrm{g}}_{\mathrm{d}}$ and $\tilde{i}^{\mathrm{g}}_{\mathrm{q}}$ are modeled by G_{11} and G_{21}. Therefore only those transfer functions are considered to validate the small-signal model. Transfer functions G_{11} and G_{21} can now be used to design the inner dq-current controller shown in Fig. 7. The controller block diagrams for d and q axis are shown in Fig. 8a and 8b, where G_{11} and G_{21} blocks represent the dynamics of Dyna-C converter.

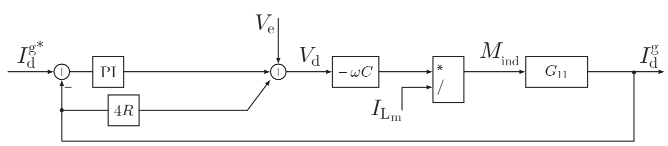

(a) d-axis controller block diagram

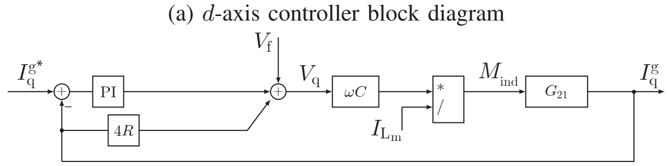

(b) q-axis controller block diagram

Fig. 8: Controller block diagrams based on small-signal plant transfer functions

V. Results and Discussion

Transfer functions G_{11} and G_{21} were calculated using MATLAB. The steady state values required in the small-signal state-space matrix (35) and input vector (37) are obtained from a simulation of the switching model with the controller shown in Fig. 7. The simulation parameters related to Fig. 1, where it is assumed that $R = R_{L_{\mathrm{a}}} = R_{L_{\mathrm{b}}} = R_{L_{\mathrm{c}}}$ and $L = L_{\mathrm{a}} = L_{\mathrm{b}} = L_{\mathrm{c}}$ are listed in Table. II. Note $\tilde{v}^{lg}_{\mathrm{grid}}$ is the line-to-ground grid voltage and the switching period is given by T_s. The bode plot and pole zero map of transfer function,

TABLE II: Simulation Parameters

Parameter	Value	Parameter	Value
v_g^{lg}	277Vrms	L	0.2mH
f_g	60Hz	C	10μ F
L_m	0.8mH	R	50mΩ
R_{dc}^{p}	15mΩ	V_{dc}	400V
ω_{res}^{11}	3.5kHz	ω_{res}^{21}	3.5kHz
n	1	T_s	100μs

G_{11} are given in Fig. 9. As expected in a fifth-order system, five poles are calculated. For the chosen operating point, it can be seen that there are two complex conjugate pole pairs and one real pole. They are all in the left half plane (LHP), which is fundamental to obtain a stable system. The resonant frequencies related to the complex conjugate pole pairs are reflected by two peaks in the bode magnitude plot. The lower resonance frequeny ω_{res}^{11} of G_{11} and ω_{res}^{21} of G_{21} are both given in Table II. The resonance frequencies of G_{11} are above 3kHz. G_{11} further contains three zeros (a complex conjugate pair and a real zero) which are all in the right half plane (RHP). The complex conjugate (RHP) zero causes the phase in Fig. 9 to be at high value of 536 degrees for low frequencies.

TABLE III: Controller Parameters

Parameter	Value	Parameter	Value
K_p^{dq}	1	K_p^{lm}	1
K_i^{dq}	30	K_i^{lm}	3

The zeros situated in the RHP underline that the Dyna-C converter is based on a flyback converter, which has a zero in the RHP [11] too. Similarly, bode plot and pole zero map for the transfer function, G_{21} are shown in Fig. 10. Since the large signal values matrix elements in (35) remain unchanged to calculate G_{21}, its eigenvalues and consequently the poles keep their values as in G_{11}, which can be seen by comparing Fig. 9 and 10. The real zero location remains unchanged while the complex conjugate zero pair moves from the RHP to LHP. The LHP zeros lead to an improvement of the phase as opposed to G_{11}, where it continuously drops. A PI controller is designed based on the switching and small-signal model simulations and the controller parameters are given in Table. III.

In order to validate the derived models, a step change was introduced to d axis and q axis current references in Fig. 8a and 8b. This is then compared to the step response from the switching model controlled by the developed controller in Fig. 7. First, the d-axis current reference is perturbed by applying a 24A $\mapsto$ 34A step to it, while the q-axis current reference is kept at zero. Simulation results are shown in Fig. 11. The switching model based d-axis current i_d^{sw} is shown by the blue plot, while the small-signal model based d-axis current i_d^{sm} is given by the red line. The small-signal model responds faster than the switching model as illustrated by Fig. 11.

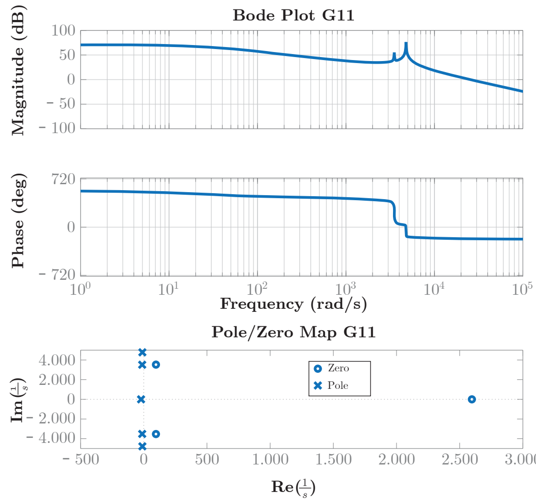

Fig. 9: Transfer function G_{11}

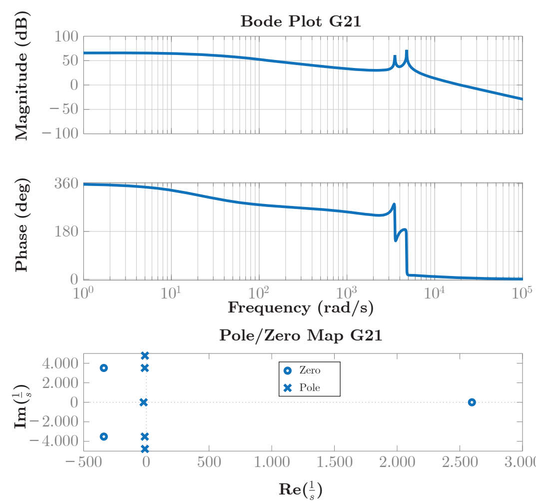

Fig. 10: Transfer function G_{21}

The same method is applied to the q-axis current reference, which is perturbed by a 0A $\mapsto$ 5A step, while i_d^g is kept at 24 A. Fig. 12 shows that the small-signal value i_q^{sm} deviates from the switching model current i_q^{sm} to a lower extent as compared to the d-axis current. The differences between the small-signal and switching model is attributed to the simplifying assumptions. In Fig. 11 and 12, only the transfer functions G_{11} and G_{21} are considered. Moreover, other terms that signify cross-coupling between the d and q axis currents are neglected. To demonstrate that the outer controller in Fig. 7 is capable in controlling the magnetizing current i_{L_m}, its step response is evaluated as well.

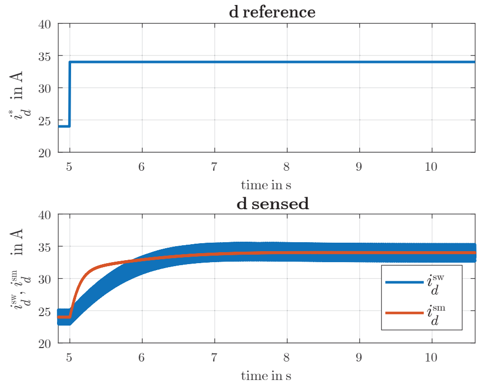

Fig. 11: Step response - d axis current.

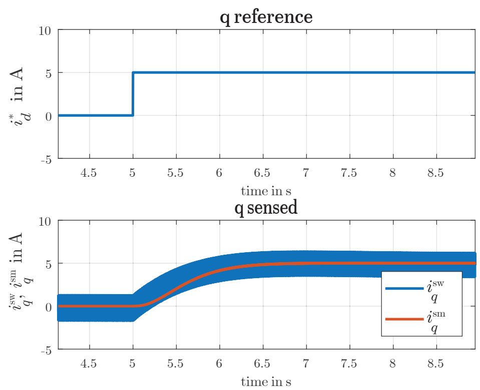

Fig. 12: Step response - q axis current.

The reference before the step, is chosen such that $i_{\mathrm{d}}^{\mathrm{g}}$ has the same value as in Fig. 11 and $i_{\mathrm{q}}^{\mathrm{g}}$ is set to zero. Simulation results are displayed in Fig. 13. The response has a slight overshoot and settles to the reference value in less than 2 seconds. Since the poles are close to the imaginary axis such a slow respance is espected. The steady state grid current and voltage waveforms are shown in Fig 14 with the chosen filtering arrangement and modulation strategy.

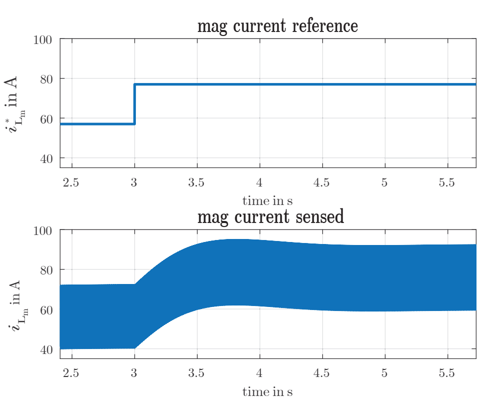

Fig. 13: Step response - magnetizing current.

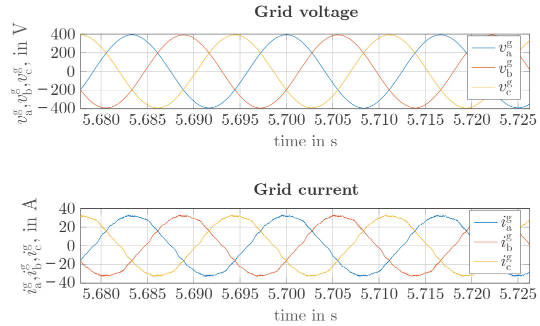

Fig. 14: Simulated grid voltage and grid current in a Dyna-C converter corresponding to steady state unity power factor operation.

VI. Conclusion

In this paper, a modulation scheme and a small-signal model for the Dyna-C ac-dc converter are proposed. The modulation scheme is developed based on the current-source characteristics and flyback nature of the Dyna-C converter. A state-space based averaging technique is used to derive the small-signal model, which is then used for designing the two loop closed-loop control structure of the Dyna-C converter. Deviations observed between the small-signal model and the switching model step responses indicate that the proposed models could be further improved. Simulation results are presented which validate the functionality of the proposed modulation and control approach.

References

[1] H. Chen, A. Prasai, R. Moghe, K. Chintakrinda, and D. Divan, “A 50 kva three-phase solid-state transformer based on the minimal topology: Dyna-c,” *IEEE Transactions of Power Electronics*, vol. 31, no. 12, p. 12, 12 2016.

[2] B. J. Baliga, *Gallium Nitride and Silicon Carbide Power Devices*. World Scientific Publishing Co. Pte. Ltd., 2017.

[3] . H. Chen, A. Prasai, and D. Divan, “Dyna-c a minimal topology for bidirectional solid-state transformers,” *IEEE*, 2017.

[4] H. Chen, A. Prasai, and D. Divan, “A modular isolated topology for instantaneous reactive power compensation,” *IEEE*, 2016.

[5] B. Mirafzal, M. Saghaleini, and A. K. Kaviani, “An svpwm- based switching pattern for stand-alone and grid-connected three phase single stage-boost inverters.” *IEEE Transactions of Power Electronics*, vol. 26, no. 4, p. 10, April 2011.

[6] R. W. D. Doncker, *Power Electronics Fundamentrals Topologies Analysis*. Institut for Power Electonics and Electrical Drives RWTH, 2014, no. ISBN 978 3 9434496 00 0.

[7] A. Moghadasi, A. Sargolzaei, M. Moghaddami, A. Sundararajan, A. Sarwat, and K. Yen, “A simplified power control approach with reliable axis decoupling capability for three-phase current source inverter,” *IEEE*, pp. 1–7, Dec 2016.

[8] A. K. Kaviani and B. Mirafzal, “Dynamic model of the three-phase single-stage boost inverter for grid-connected applications,” *IEEE*, pp. 4627–4634, Sept 2012.

[9] MathWorks, “Mathworks documentation abc to dqo and dq0 to abc,” https://ch.mathworks.com/help/physmod/sps/powersys/ref/abctodq0dq0toabc.html, 2013.

[10] M. W. Y. Chen, “A fast pll method for power electronic systems connected to distorted grids,” *IEEE*, 2007.

[11] H. Terashi, I. Cohen, and T. Ninomiya, “Stability and dynamic response improvement of flyback dc-dc converter by a novel control scheme,” *IEEE*, vol. 1, pp. 389–394 vol.1, 2002.